Mammographic Images Enhancement and Denoising for Breast Cancer Detection Using Dyadic Wavelet Processing

Arianna Mencattini, *Member, IEEE*, Marcello Salmeri, *Member, IEEE*, Roberto Lojacono, Manuela Frigerio, and Federica Caselli

***Abstract*—Mammography is the most effective method for the early detection of breast diseases. However, the typical diagnostic signs such as microcalcifications and masses are difficult to detect because mammograms are low-contrast and noisy images. In this paper, a novel algorithm for image denoising and enhancement based on dyadic wavelet processing is proposed. The denoising phase is based on a local iterative noise variance estimation. Moreover, in the case of microcalcifications, we propose an adaptive tuning of enhancement degree at different wavelet scales, whereas in the case of mass detection, we developed a new segmentation method combining dyadic wavelet information with mathematical morphology. The innovative approach consists of using the same algorithmic core for processing images to detect both microcalcifications and masses. The proposed algorithm has been tested on a large number of clinical images, comparing the results with those obtained by several other algorithms proposed in the literature through both analytical indexes and the opinions of radiologists. Through preliminary tests, the method seems to meaningfully improve the diagnosis in the early breast cancer detection with respect to other approaches.**

***Index Terms*—Dyadic wavelet transform, image enhancement and denoising, mass detection, microcalcification detection.**

I. Introduction

BREAST cancer is the leading cause of death among women. The *National Cancer Institute* estimates that one out of eight women in the United States will develop breast cancer at some point during her lifetime [1]. Primary prevention seems impossible because the causes of this disease still remain unknown. Early detection is the key to improving breast cancer prognosis.

X-ray mammography is the most common technique used by radiologists in the screening and diagnosis of breast cancer. Although it is seen as the most reliable method for early detection of breast carcinomas, reducing mortality rates by up to 25%, its interpretation is very difficult—10%–30% of breast lesions are missed during routine screening [2], [3].

Manuscript received July 15, 2006; revised November 8, 2007. This work was supported, in part, by the Telesal Project.

A. Mencattini, M. Salmeri, R. Lojacono, and M. Frigerio are with the Department of Electronic Engineering, University of Rome "Tor Vergata," 00133 Rome, Italy (e-mail: mencattini@ing.uniroma2.it; salmeri@ing.uniroma2.it; lojacono@ing.uniroma2.it).

F. Caselli is with the Department of Civil Engineering, University of Rome "Tor Vergata," 00133 Rome, Italy (e-mail: caselli@ing.uniroma2.it).

Digital Object Identifier 10.1109/TIM.2007.915470

To increase the diagnostic performance of radiologists, several computer-aided diagnosis schemes have been developed to improve the detection of either of the two primary signatures of this disease: 1) masses and 2) microcalcifications.

Masses are defined as space-occupying lesions that are described by their shapes and margin properties. A benign neoplasm is smoothly marginated, whereas a malignancy is characterized by an indistinct border that becomes more spiculated with time. Because of the slight differences in the X-ray attenuation between masses and benign glandular tissue, they appear with low contrast and are often very blurred. Microcalcifications are tiny deposits of calcium that appear as small bright spots in the mammogram. Although they have higher inherent attenuation properties, they cannot be distinguished from the high-frequency noise because of their small size. The average size of microcalcifications is about 0.3 mm. Thus, the relevant features involved are variability, occurrence at different scales and orientations, and characterization by discontinuous changes in intensity, as well as more subtle global variations in texture.

Wavelet processing is extremely necessary when the analysis of a multiscale feature is important. In fact, when using the wavelet transform, it is possible to detect details that appear at different scales and selectively enhance them within different resolution levels.

In particular, wavelet orthogonal and biorthogonal bases have been successfully used in many applications. It has already been stressed that the lack of translation invariance of these representations can be a severe drawback because this leads to the introduction of a large number of artifacts in the reconstruction after the processing of the wavelet coefficients. We refer, for example, to the pseudo-Gibbs phenomena in the neighborhood of discontinuities [4]. The *dyadic wavelet transform* [5]–[8] pioneered by Mallat and Zhong was precisely introduced to cope with this. It provides a redundant representation so that it exhibits translation invariance, and in [9], it was shown that by using an undecimated transform rather than a decimated one, it can improve the results of denoising by more than 2.5. This undecimated decomposition is computed using the same filter bank of a biorthogonal wavelet transform, and each band has the same size as the original image.

The general scheme for a wavelet-based image enhancement is the following: 1) wavelet decomposition; 2) modification of wavelet coefficients at various scales; and 3) image reconstruction starting from modified coefficients. In this paper, we use, as

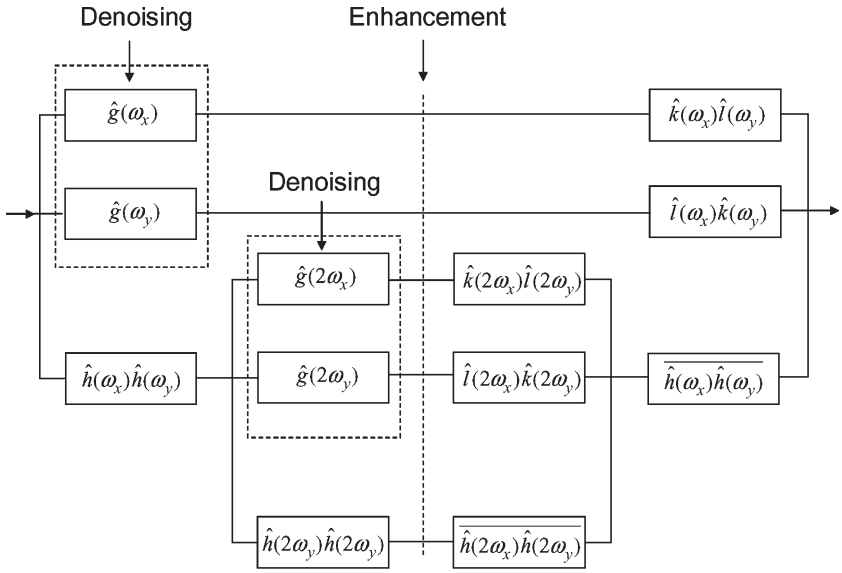

Fig. 1. Two-dimensional dyadic wavelet transform (two levels shown).

a redundant representation, the discrete dyadic transform introduced in [5], which can be implemented within the hierarchical filtering scheme shown in Fig. 1, in which the points at which the denoising and enhancement are inserted are highlighted. Filter definition can be found in [6]–[8].

The paper is organized as follows. In Section II, the foundation of the used methodology using the particular class of undecimated wavelets is shown. Sections III and IV describe how this approach has been applied in the case of mammographic images to extract microcalcifications and masses, respectively. Section V explains the comprehensive algorithm that allows us to identify both microcalcifications and masses by using the same core of the algorithm. Finally, in Section VI, the results achieved by using the proposed algorithms are presented and discussed.

II. Wavelet Shrinkage Denoising

Any real signal is corrupted by some noise. Because the presence of noise could disturb the processing in the wavelet domain and frustrate the enhancement operation, it is first necessary to denoise the data.

However, conventional filtering techniques cannot be applied in the context of medical imaging because they produce edge blurring and loss of details. To achieve edge-preserving filtering, we apply the well-known wavelet shrinkage denoising [10] on the output coefficients of filters $\hat{g}(\cdot_x)$ and $\hat{g}(\cdot_y)$. Two classes of filters are possible: 1) gradient and 2) Laplacian filters. The first kind is more suitable when using denoising operation because gradient coefficients exhibit higher signal-to-noise ratios with respect to Laplacian ones.

As noted in [11], if the two oriented wavelet coefficients are independently processed, orientation distortions are introduced; thus, the magnitude M of these coefficients must be considered. The following shrinking operator is used:

$$C(M) = \begin{cases} |M| - T_n, & |M| \geq T_n \\ 0, & \text{otherwise.} \end{cases}$$

Note that this operator is a monotonically nondecreasing function to avoid the introduction of artifacts.

The key issue is the optimal selection of the threshold T_n. A threshold that is too large produces blurring of small edges, whereas a low one does not remove enough noise.

In [11], a connection is proved between T_n and the parameter η of a Rayleigh distribution. In a previous paper [12], we proved that, given two Gaussian random variables X and Y with zero mean and variance σ^2, the variable $Z = \sqrt{X^2 + Y^2}$ has a Rayleigh probability density function (pdf) with

$$\eta = \sigma. \tag{1}$$

The proof of this relation is in the Appendix. It follows that

$$f(Z) = \begin{cases} \frac{Z}{\sigma^2} e^{-(Z/\sigma)^2/2}, & Z \geq 0 \\ 0, & \text{otherwise.} \end{cases}$$

Provided that we are able to correctly estimate the noise variance σ, it is possible to tune T_n using

$$T_n = \sigma\sqrt{-2\log(1-p)}$$

where p is the probability of achieving a correct value.

The noise variance estimation is obtained through a local iterative fuzzy method described in [13] and [14]. This algorithm is an iterative procedure tuned by a regression analysis that is based on fuzzy processing. This processing is applied to some properties of the image, such as the matching between the theoretical luminance distribution and the local one. The basic idea is to give more importance, in the variance computation, to those windows of the image that present a uniform distribution and whose variance consequently correspond with the noisy one.

Fig. 2 shows the whole denoising procedure where FNVE stands for *fuzzy noise variance estimator*, which is cited above.

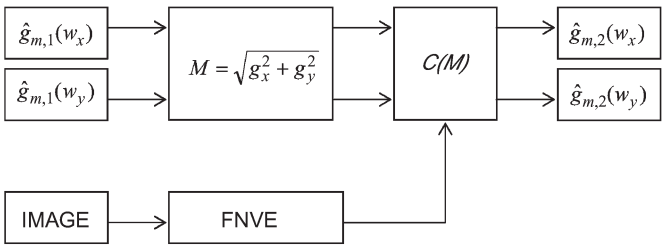

Fig. 2. Denoising with adaptive threshold estimation.

III. Microcalcifications Detection

In this section, we describe a general method to accomplish multiscale contrast enhancement. In the wavelet framework, linear and nonlinear enhancement operators have been proposed in the literature. Linear enhancement can be seen as a mapping of wavelet coefficients by a linear function $E_m = G_m\, s$, where s denotes each wavelet coefficient, and the gain G_m is, in general, level dependent. In [11], Fan and Laine proved that linear enhancement corresponds to unsharp masking incorporated at each scale.

To avoid the saturation of high-value coefficients, which causes loss of details after the reconstruction process, the use of a nonlinear enhancement is needed. Unfortunately, designing a nonlinear enhancement function is a nontrivial task, and one has to take into account the following constraints. First, the nonlinear function $E_m(s)$ has to be monotonically increasing so that no artifacts are introduced during the processing and the reconstruction. Moreover, an area of low contrast has to be enhanced more than an area of high contrast so that the saturation effects can be minimized after the rescaling procedure. Finally, a sharp edge should not be blurred. Following these considerations, in [11], Fan and Laine proposed a nonlinear piecewise mapping $E_m(s)$ of the form

$$E_m(s) = \begin{cases} s - (G_m - 1)T, & s < -T \\ G_m\, s, & |s| \le T \\ s + (G_m - 1)T, & s > T. \end{cases}$$

Because the choice of the parameters G_m and T_m defines the boundary between the hard enhancement (slope G_m) and the soft enhancement (unitary slope), it represents a critical step in the procedure. To make efficient use of the multichannel information from a dyadic wavelet framework, these parameters should be adaptively chosen. In [11], T_n is selected as $t \cdot \max\{|l_x + l_y|\}$, where $t \in [0, 1]$ is user specified. In these kinds of images, the best value for parameter t is equal to 0.1, as pointed out in [11], to discriminate as much as possible the coefficients to be enhanced to maximize the image contrast.

In [12], we have proposed a new algorithm to also select the gain G_m, depending on the resolution level. In fact, if the gain is fixed across scales, a very high value of a coefficient at the first level can cause the underenhancement of coefficients at deeper levels. We applied a proper normalization to adequately enhance the coefficients at the same position at deeper levels. Through this normalization, the gain G_m is selected at each scale to satisfy the following condition: $G_m \cdot \max\{|l_x(m) + l_y(m)|\} = \text{const} = G_0 \cdot T_{\max}$, where $T_{\max} = \max_m\{|l_x(m) + l_y(m)|\}$, and G_0 is user defined. In our case, G_0 has been chosen equal to 12 because larger values produce excessive saturation in the image under analysis.

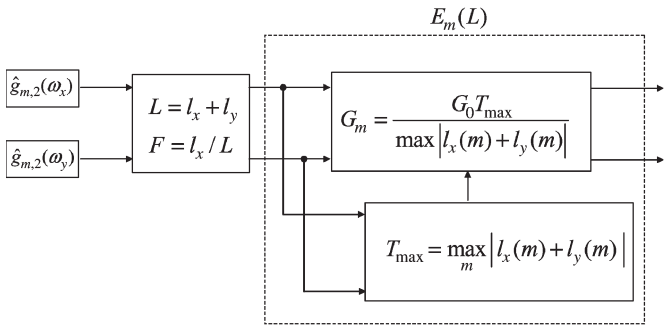

Fig. 3. Adaptive gain setting.

Fig. 3 shows this procedure for level m. Note that l_x and l_y are the output coefficients of filters $\hat{g}(\cdot_x)$ and $\hat{g}(\cdot_y)$. However, enhancement operation is better performed on Laplacian coefficients. Thus, we split the Laplacian operator at a generic level m into two cascaded gradient operators $\hat{g}_{m,1}(\cdot)$ and $\hat{g}_{m,2}(\cdot)$. We insert the denoising step after the first one and the enhancement step after the second one.

As an illustrative example, consider a three-level decomposition of a 1-D signal $y = f(x)$, which can be seen as a single line of an image, shown in Fig. 4. Fig. 4(a) represents the case $G_m = G_0$ for three levels, whereas Fig. 4(b) represents the effects of adaptively setting G_m.

IV. Mass Detection

Mass enhancement introduces much more difficult problems with respect to microcalcifications. In fact, because of low contrast, they appear embedded in and camouflaged by varying densities of parenchymal tissue structures. Thus, it is very difficult not only to visually detect them on mammograms but also to distinguish, in the wavelet domain, the coefficients related to suspicious masses from the ones related to the background. To operate a selective enhancement of the relevant features, a segmentation of the image is required.

A. Segmentation

Image segmentation techniques may be classified into two main groups, depending on the approach of the concerned algorithm: 1) discrete contour models and 2) region growing. The first are based on edge-detection techniques. An edge image shows each object in edge points that have to be linked to obtain the close connected boundaries that are required for image segmentation, but the result of edge-point linking is not exact. On the contrary, in region growing methods, the region is generally set in advance; thus, this algorithm is poor when the object outline has a random shape. In this paper, we introduce a new method of segmentation that effectively combines both information concerning the boundaries and the core of image structures.

Multiscale edge detection is related to the wavelet transform. In [5], Mallat and Zhong show that a Canny edge detector is

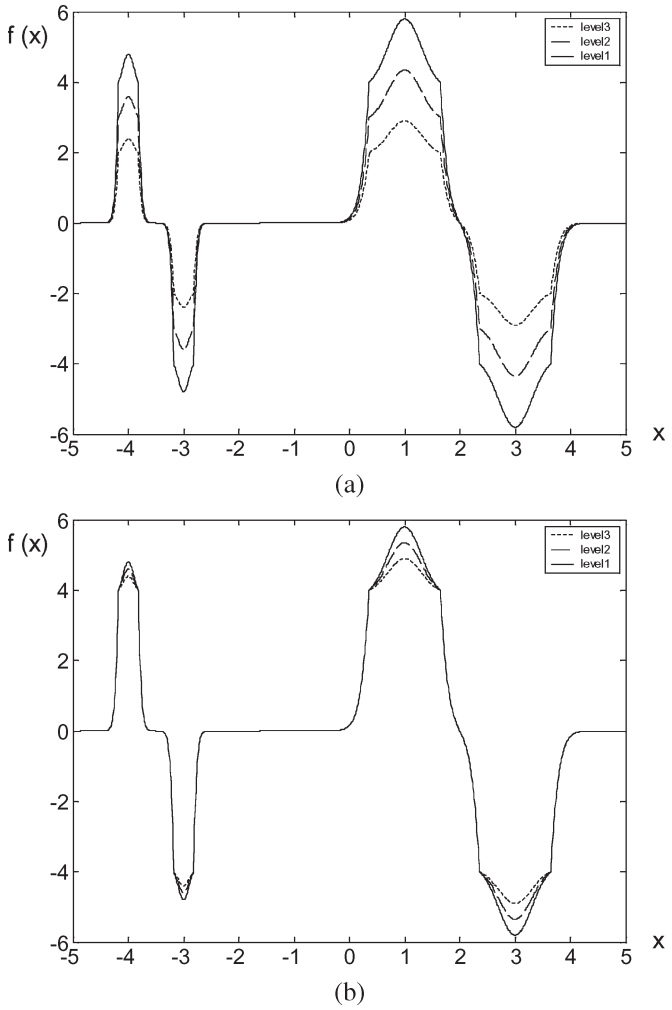

Fig. 4. Effect of adaptive gain on a 1-D signal $y = f(x)$.

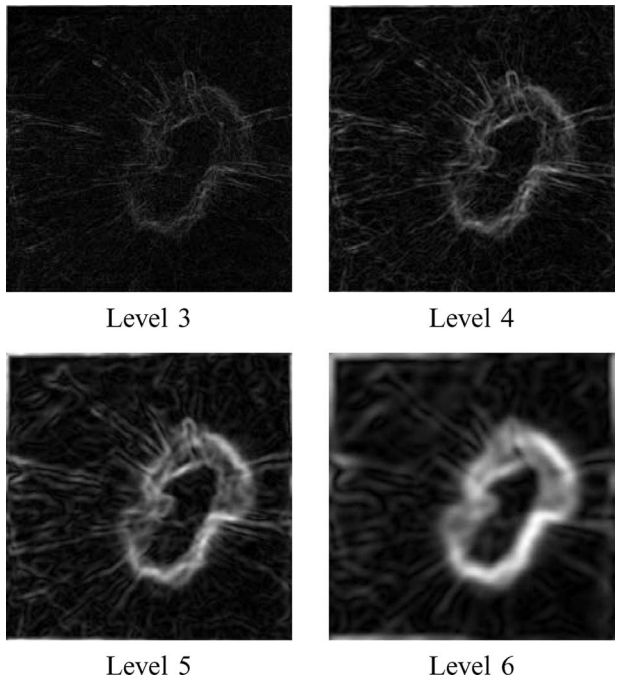

Fig. 5. Example of the image details for the different decomposition levels.

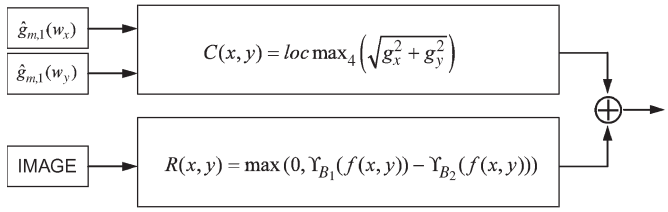

Fig. 6. Segmentation algorithm scheme.

equivalent to finding the local maxima of a wavelet transform modulus. In particular, when the scale is large, the transformation removes small signal fluctuations so that it is possible to detect only the sharp variations of large structures. Several simulations have proved that the fourth-level decomposition band is the best choice for mass boundaries revealing. The example in Fig. 5 shows how the decomposition level affects, in these kinds of images, the details that can be revealed by justifying the choice of the fourth level.

However, the dyadic scales are not sufficient for the detection of masses in mammograms. As noted in [15], a lesion may be too blurred on one scale and too fragmented on the next. Therefore, we need further information concerning the mass core by using a different approach. We design a background-removal algorithm based on the properties of morphological filters, which are also used in [16], as shown in Fig. 6.

Morphological filters are nonlinear signal transformations that locally modify the geometric features of signals. The force of the mathematical morphology approach comes from the fact that a large class of filters can be represented as the combination of two simple operations: 1) *erosion and* 2) *dilation*. Let Z denote the set of integers and $f(x, y)$ is a discrete image signal whose domain set is given by $\{x, y \in N_1 \times N_2\}$, where N_1, $N_2 \subset Z$. A structuring element B is a subset in Z^2 with a simple geometrical shape. The erosion and dilation can be expressed as

$$(f \ominus B)(x, y) = \max\{f(x - t_1, y - t_2), (t_1, t_2) \in B\}$$

$$(f \oplus B)(x, y) = \max\{f(x + t_1, y + t_2), (t_1, t_2) \in B\}$$

respectively. On the other hand, the opening and closing are defined as

$$(f \circ B)(x, y) = [(f \ominus B) \oplus B](x, y)$$

$$(f \bullet B)(x, y) = [(f \oplus B) \ominus B](x, y).$$

Given an image, the opening operation removes the objects having sizes that are smaller than the structuring element. Thus, with a specified structuring element, one can extract different image contexts by taking the difference between the original image and the one processed by the opening operator, which is a process called *tophat operation*. The algorithm is implemented by dual morphological tophat operations followed by a subtraction that is described as follows.

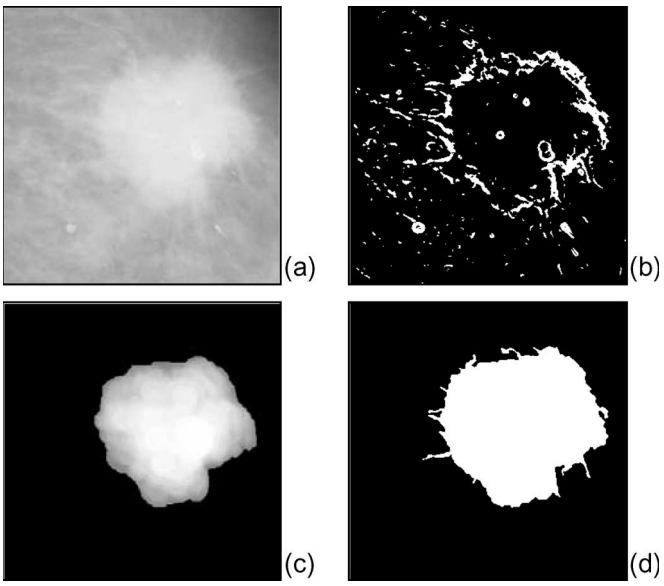

Fig. 7. Segmentation steps. (a) Original mammogram. (b) Effect of gradient processing. (c) Image after the morphological filtering procedure. (d) Final segmented mammogram.

The textures without diagnostic relevant contents are extracted by a tophat operation

$$\Upsilon_{B_1}[f(x,y)] = \max[0, f(x,y) - (f \circ B_1)(x,y)]$$

where Υ_{B_1} denotes the tophat operation between the original image $f(x,y)$ and a specified structuring element B_1, whose size should be chosen smaller than the size of masses.

Let Υ_{B_2} be the mass pattern-enhanced image by background correction by the second tophat operation

$$\Upsilon_{B_2}[f(x,y)] = \max[0, f(x,y) - (f \circ B_2)(x,y)]$$

where B_2 is a specified structuring element that has a larger size than mass.

Obviously, the value for B_1 and B_2 depends on the image resolution. In our case, because the mammogram images have a resolution equal to 40 μm, these values have been tuned to 36 and 180, respectively.

The resulting image $R(x,y)$ can be derived as

$$R(x,y) = \max(0, \Upsilon_{B_2} - \Upsilon_{B_1}).$$

Fig. 7 shows the result of each segmentation step.

B. Enhancement

Because we have obtained the segmentation of the mammographic image, we can use the resulting binary image denoted as $S(x,y)$ as a sort of map to operate a selective enhancement in the wavelet domain. Only wavelet coefficients corresponding to the segmented mass are enhanced and thus multiplied for a user-defined gain G_0

$$E_m[s(x,y)] = \begin{cases} G_0\, s(x,y), & S(x,y) = 1 \\ s(x,y), & S(x,y) = 0. \end{cases}$$

V. Whole Algorithm

To summarize the whole algorithm for both microcalcification and mass lesion processing in Fig. 8, we will denote with a solid line the block diagram for the microcalcification enhancement and denote with a dashed line the block diagram for the mass lesion enhancement. Note that the core of the processing, which is represented by the wavelet decomposition, the enhancement, and the wavelet reconstruction, are the same, whereas the main differences are principally due to the level selection and segmentation blocks. Level selection allows wavelet coefficient processing performing a level discrimination so that different weights are applied to different levels. Segmentation is only applied to mass detection to implement a selective enhancement based on the mask provided by the segmentation itself.

This figure highlights the main advantage of the proposed algorithm, which is the ability of using the same computation core for both microcalcifications and mass detection. This is a great advantage, considering the next objective of the research, which is the hardware field-programmable gate array implementation of the algorithm to realize a very fast but inexpensive system to provide real-time processing of the acquired images.

VI. Results and Discussion

The described method has been tested on many mammographic images taken from the Digital Database for Screening Mammography (DDSM) at the University of South Florida, Tampa [17]. The primary purpose of this database is to facilitate a sound research in the development of computer algorithms to aid in screening. The database approximately contains 2500 studies, and each study includes two images [lossless Joint Photographers Expert Group (LJPEG) format, gray coded, with 12- or 16-bit pixel depth] of each breast, along with some associated patient information [age at the time of study, an American College of Radiology (ACR) breast density rating, subtlety rating for abnormalities, an ACR keyword description of abnormalities] and image information (scanner, spatial resolution, and so on). Images containing suspicious areas have associated pixel-level "ground truth" information about the locations and types of suspicious regions.

The information provided by the radiologists and their opinions are the main sources to validate the algorithm. Thus, the achieved results have been compared with those provided by the DDSM and, moreover, have always been submitted to the assessment of several specialists.

In particular, all the microcalcifications identified by the specialists in the database (many of them classified with a very high subtlety rating) have been correctly enhanced by the algorithm without the introduction of any artifact, allowing a more simple detection by the radiologist with respect to the plain image or the image processed by standard algorithms.

Fig. 9 shows the region of interest (ROI) of an original dense mammographic image with a microcalcification lesion with a linear distribution and an oval-shaped mass lesion with margins ill-defined. One can notice the disastrous effects of the

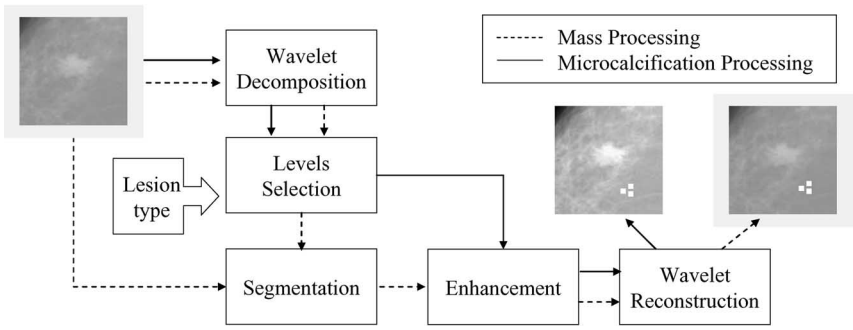

Fig. 8. Whole algorithm involving both microcalcifications and mass detection.

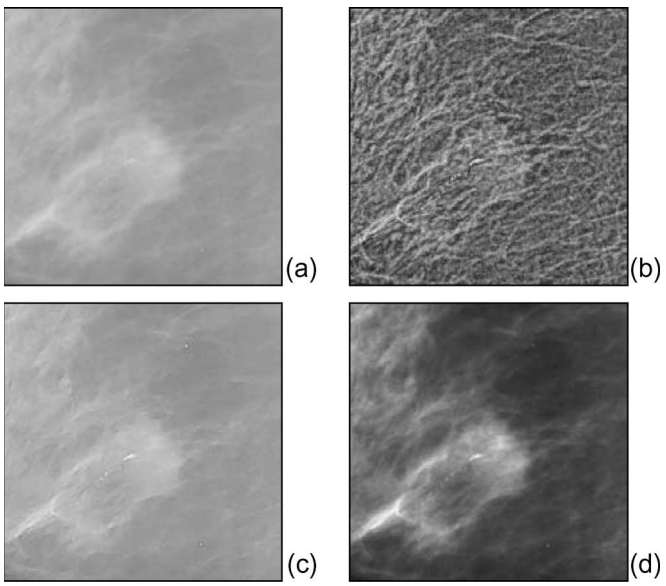

Fig. 9. Microcalcification detection. (a) Original mammogram. (b) Enhancement without denoising. (c) Piecewise linear enhancement in range [0, 1]. (d) Maximum visualization range.

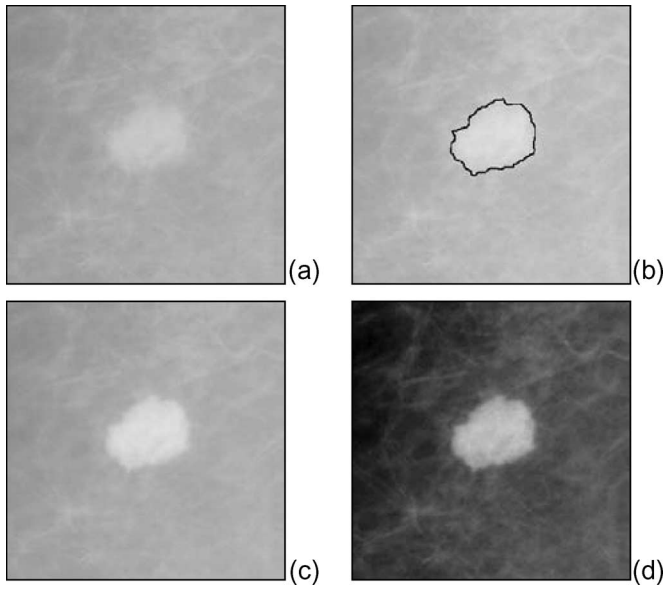

Fig. 11. Mass detection. (a) Original mammogram. (b) Boundaries of the segmented mass. (c) Enhanced mammogram in range [0, 1]. (d) Maximum visualization range.

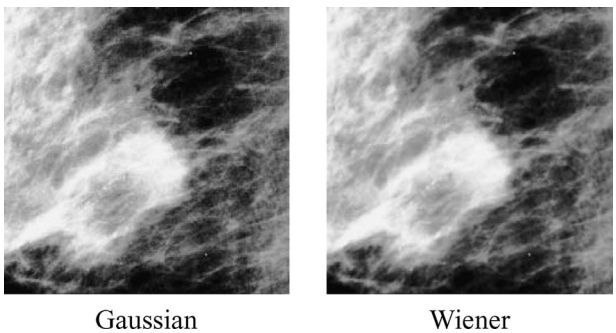

Fig. 10. Denoising of the mammographic image by two classical algorithms.

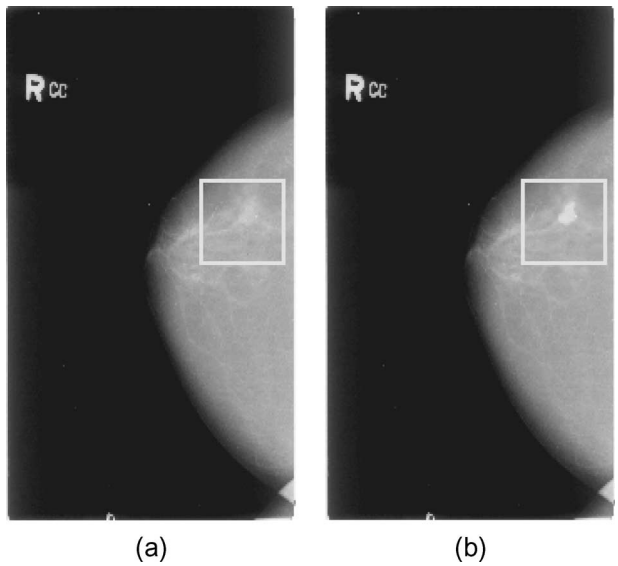

Fig. 12. Effect of the enhancement procedure on the whole mammogram. (a) Original mammogram, which indicates the ROI containing the mass lesion. (b) Processed image in which the mass lesion appears enhanced and much more recognizable.

application of the enhancement without denoising. On the contrary, after the denoising step, the piecewise operator makes the microcalcifications more visible than the margins of the mass. The same image processed by two other classical algorithms is shown in Fig. 10. One can notice how these algorithms fail because of the particular nature of these noisy images having very low contrast.

Regarding the mass detection, Fig. 11 shows an example of mass segmentation and enhancement algorithm. We note that, through segmentation, it is possible to correctly highlight the

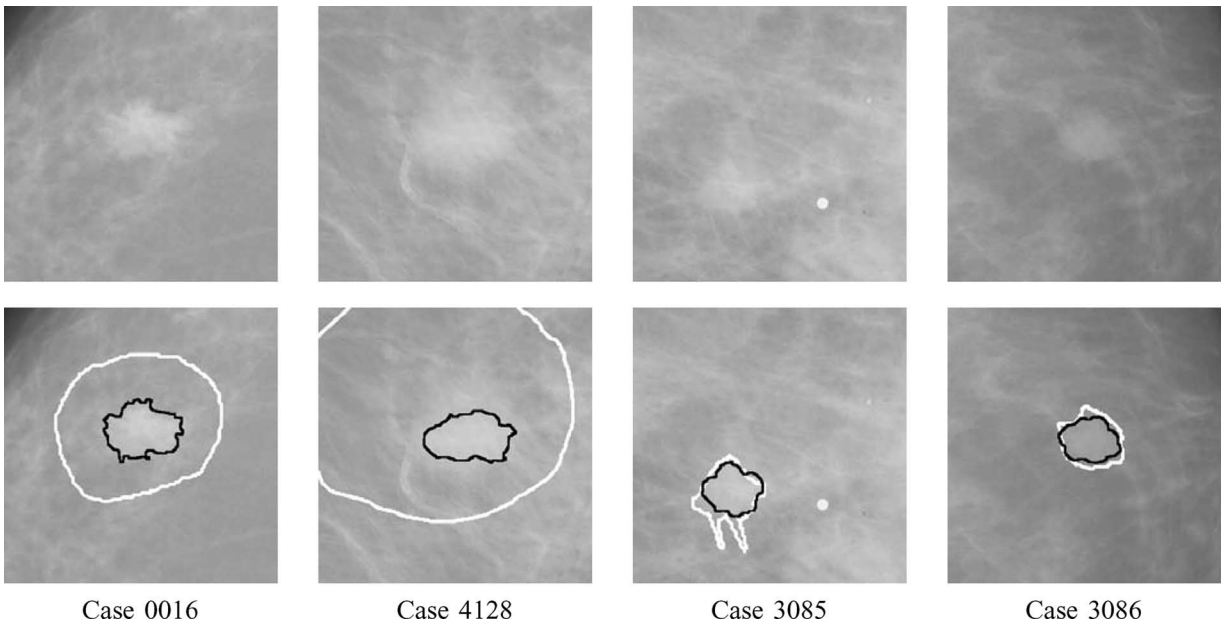

Fig. 13. Comparison between the mass edge identified by the radiologist (white line) and that detected by the algorithm (black line).

proper boundaries of the mass lesion and enhance it without emphasizing the background structures.

In Fig. 12, it is also shown that this procedure provides a significant improvement in the image quality, even on the whole mammographic image.

The performance evaluation of a mass lesion should take into account both the lesion identification and its correct edge detection. This last characteristic indeed allows the radiologist to understand the true nature of the lesion.

In the DDSM database, these kinds of lesions are identified by the specialists either

a) by a circle around the lesion or
b) by its edge contour.

In case b), in which the specialist outlined the contour of the mass, the performance of the algorithm can be evaluated by the ratio of the mutual overlap area of the radiologist-segmented mass region and the algorithm-segmented mass region to the radiologist-segmented mass [18]. Typically, this ratio should be greater than 0.5.

Our preliminary tests, carried out on 106 images, show that in case a), the mass lesion is always correctly identified (the area bounded by the edge totally lies into the circle), whereas in case b), the overlapping index is always much larger than 0.5, with the mean value equal to 0.8 (with a standard deviation equal to 0.15). Moreover, several radiologists declared that the shape of the contour is very precise, and it permits a very simple and safe classification of the mass.

Fig. 13 shows some examples of the algorithm results, identified by the case number in the figure labels. The top figure represents the original image, whereas the bottom figure depicts the comparison between the mass edge identified by the radiologist (white line) and detected by the algorithm (black line). In particular, in the first two cases, the radiologist identified the mass by a circle, and the computerized edge is contained inside this circle. Moreover, one can notice that this contour exactly matches the mass shape. In the last two examples, in which the specialist contour has been outlined following the mass lesion shape, the computerized edge is very close to the edge identified by the radiologist.

VII. Conclusion

In this paper, we have addressed the problem of enhancement and denoising of mammographic images.

A new algorithm based on the dyadic wavelet transform has been presented. The main advantage of this method, with respect to the other methodologies proposed in the literature, is its adaptability to the different nature of diagnostic relevant features in the image under analysis, permitting the use of the same core algorithm for both microcalcifications and mass detection.

Many simulation results prove the suitability of this approach to enhance both very small features, such as microcalcifications, and very low-contrast structures, such as masses. The improving quality of the processed images has been considered by radiologists as a true significant aid for the early detection of breast cancer.

Future development of the presented research concerns the improvement of the whole procedure performance through a fine tuning of the algorithm parameters according to the peculiarities of the image under analysis. In particular, a new signal-dependent algorithm for image noise estimation [19], developed by the same research group, has been recently tuned, particularly for mammographic images. The new algorithm will be included in the denoising procedure. Moreover, an automatic classification procedure is under development [20] to attend the radiologist in the decision phase.

Furthermore, the design of the algorithm goes toward the hardware implementation of the heavy core of the wavelet computation, permitting the realization of a real-time processing

of the image. A preliminary synthesis of the core has been proposed in [21].

APPENDIX
PROOF OF RELATION (1)

Denoting with

$$E[Z] = \int_{-\infty}^{\infty} Z f_Z(Z) dZ$$

the expected value of the random variable Z, where $f_Z(Z)$ is the pdf of Z, we have

$$E[Z] = E\left[\sqrt{X^2 + Y^2}\right]$$

and consequently

$$E[Z^2] = E[X^2 + Y^2] = E[X^2] + E[Y^2]$$

from the linearity of the operator $E[\cdot]$. Remember that

$$\sigma_X^2 = E[X^2] - E^2[X]$$

and because X and Y are zero mean random variables, it follows that

$$E[X^2] = \sigma_X^2$$

$$E[Y^2] = \sigma_Y^2.$$

Thus, we have

$$E[Z^2] = \sigma_X^2 + \sigma_Y^2 = 2\sigma^2.$$

Now, recalling that [22]

$$E[Z] = \sqrt{\frac{\pi}{2}}\eta$$

$$\sigma_Z^2 = 2\eta^2\left(1 - \frac{\pi}{4}\right)$$

it follows that

$$E[Z^2] = \sigma_Z^2 + E[Z^2] = 2\eta^2\left(1 - \frac{\pi}{4}\right) + \frac{\pi}{2}\eta^2 = 2\eta^2$$

and so

$$\sigma = \eta.$$

ACKNOWLEDGMENT

The authors would like to thank G. Rabottino, S. Romano, M. Arnò, and F. Martini of the Department of Electronic Engineering, University of Rome "Tor Vergata," Rome, Italy, for their substantial contribution to the simulation of many mammographic images and to the development of several procedures during their theses. The authors would also like to thank K. Krish of the Department of Electrical and Computer Engineering, North Carolina State University, Raleigh, for his useful contribution to LJPEG decoding procedures.

REFERENCES

[1] L. M. Wun, R. M. Merril, and E. J. Feuer, "Estimating lifetime and age-conditional probabilities of developing cancer," *Lifetime Data Anal.*, vol. 4, no. 2, pp. 169–186, Jun. 1998.

[2] C. J. Baines, D. V. McFarlane, and A. B. Miller, "The role of the reference radiologist. Estimates of inter-observer agreement and potential delay in cancer detection in the national breast screening study," *Invest. Radiol.*, vol. 25, no. 9, pp. 971–976, Sep. 1990.

[3] M. G. Wallis, M. T. Walsh, and J. R. Lee, "A review of false negative mammography in a symptomatic population," *Clin. Radiol.*, vol. 44, no. 1, pp. 13–15, Jul. 1991.

[4] R. R. Coifman and M. V. Wickerhauser, "Entropy-based algorithms for best basis selection," *IEEE Trans. Inf. Theory*, vol. 38, no. 2, pp. 713–718, Mar. 1992.

[5] S. Mallat and S. Zhong, "Characterization of signals from multiscale edges," *IEEE Trans. Pattern Anal. Mach. Intell.*, vol. 14, no. 7, pp. 710–732, Jul. 1992.

[6] M. J. Shensa, "The discrete wavelet transform: Wedding the à trous and Mallat algorithms," *IEEE Trans. Signal Process.*, vol. 40, no. 10, pp. 2464–2482, Oct. 1992.

[7] S. Mallat, "A theory for multiresolution signal decomposition: The wavelet representation," *IEEE Trans. Pattern Anal. Mach. Intell.*, vol. 11, no. 7, pp. 674–693, Jul. 1989.

[8] S. Mallat, *A Wavelet Tour of Signal Processing*. San Diego, CA: Academic, 1998.

[9] J. L. Starck, M. Elad, and D. Donoho, "Redundant multiscale transforms and their application for morphological component analysis," *Adv. Imaging Electron Phys.*, vol. 132, pp. 287–348, 2004.

[10] D. L. Donoho, "De-noising by soft-thresholding," *IEEE Trans. Inf. Theory*, vol. 41, no. 3, pp. 613–627, May 1995.

[11] J. Fan and A. Laine, "Contrast enhancement by multiscale and nonlinear operators," *Wavelets in Medicine and Biology*. Boca Raton, FL: CRC, Mar. 1996, pp. 163–192.

[12] A. Mencattini, M. Salmeri, R. Lojacono, and F. Caselli, "Mammographic images enhancement and denoising for microcalcification detection using dyadic wavelet processing," in *Proc. Intrum. Meas. Technol. Conf.*, Apr. 2006, vol. 1, pp. 49–53.

[13] M. Salmeri, A. Mencattini, E. Ricci, and A. Salsano, "Noise estimation in digital images using fuzzy processing," in *Proc. IEEE Int. Conf. Image Process.*, Thessaloniki, Greece, Oct. 2001, pp. 517–520.

[14] A. Mencattini, M. Salmeri, S. Bertazzoni, and A. Salsano, "Noise variance estimation in digital images using iterative fuzzy procedure," *WSEAS Trans. Syst.*, vol. 4, no. 2, pp. 1048–1056, Oct. 2003.

[15] V. Laffont, F. Durupt, M. A. Birgen, S. Bauduin, and A. F. Laine, "Detection of masses in mammography through redundant expansion of scales," in *Proc. 23th Annu. EMBS Int. Conf.*, Istanbul, Turkey, Oct. 2001, vol. 1.

[16] A. Mencattini, M. Salmeri, R. Lojacono, S. Romano, and G. Rabottino, "Breast cancer segmentation by means of wavelet analysis and morphological operators," in *Proc. Eur. Conf. Med. Phys.*, Castelvecchio Pascoli, Italy, Sep. 2007.

[17] Univ. South Florida, "Univ. South Florida digital mamonography home page," 2000.

[18] H. Li, Y. Wang, K. J. Ray Liu, S.-C. B. Lo, and M. T. Freedman, "Computerized radiographic mass detection—Part I: Lesion site selection by morphological enhancement and contextual segmentation," *IEEE Trans. Med. Imag.*, vol. 204, no. 4, pp. 289–301, Apr. 2001.

[19] A. Mencattini, M. Salmeri, R. Lojacono, and M. Arnò, "Noise estimation in mammographic images for adaptive denoising," in *Proc. Eur. Conf. Med. Phys.*, Castelvecchio Pascoli, Italy, Sep. 2007.

[20] A. Mencattini, M. Salmeri, R. Lojacono, G. Rabottino, and S. Romano, "Mammographic image analysis for tumoral mass automatic classification," in *Proc. Eur. Conf. Med. Phys.*, Castelvecchio Pascoli, Italy, Sep. 2007.

[21] M. Salmeri, S. Bertazzoni, F. Martini, and A. Mencattini, "FPGA implementation of a fast hardware architecture for medical digital image processing," in *Proc. Eur. Conf. Med. Phys.*, Castelvecchio Pascoli, Italy, Sep. 2007.

[22] A. Papoulis, *Probability, Random Variables, and Stochastic Processes*, ser. Electrical Engineering Series. New York: McGraw-Hill, May 1991.

Arianna Mencattini (S'01–M'05) was born in Rome, Italy, on July 17, 1974. She received the Dr.Eng. degree (*summa cum laude*) in electronic engineering and the Ph.D. degree in electronic engineering from the University of Rome "Tor Vergata," in 2000 and 2004, respectively.

She is currently a Researcher with the Department of Electronic Engineering, University of Rome "Tor Vergata." Her research interests include signal and image measurements and processing, noise estimation, and fuzzy theory and applications.

Marcello Salmeri (S'84–M'90) was born in Rome, Italy, on June 27, 1963. He received the Dr.Eng. degree in electronic engineering and the Ph.D. degree in electronic engineering from the University of Rome "Tor Vergata," in 1989 and 1993, respectively.

He is currently an Associate Professor with the Department of Electronic Engineering, University of Rome "Tor Vergata." His research interests include signal and image processing, theory, applications, and implementations of fuzzy systems, pattern recognition, and evolutionary algorithms for systems optimization.

Roberto Lojacono was born in Palermo, Italy, on February 2, 1941. He received the Bachelor's degree in physics from the University of Catania, Catania, Italy, in 1966.

In 1976, he was a Lecturer with the Faculty of Engineering Faculty, University of Rome "La Sapienza," Rome, Italy, where he became an Associate Professor in 1993 and a Full Professor in 1990. Until 1983, he was also a Teacher with an Italian High School. He was an Invited Professor with the Ecole Polytechnique Federale de Lausanne, Lausanne, Switzerland, in 1984 and 1988. He is currently with the Department of Electronic Engineering, University of Rome "Tor Vergata." His research interests include nonlinear circuit analysis, fuzzy logic, finite arithmetic, signal measurements, signal processing, and related VLSI design.

Manuela Frigerio was born in Giussano, Milan, Italy, on August 15, 1981. She received the Laurea degree (*summa cum laude*) in electronic engineering from the University of "Tor Vergata," Rome, Italy, in 2006.

She is currently with the Department of Electronic Engineering, University of Rome "Tor Vergata."

Federica Caselli was born in Rome, Italy, on October 27, 1981. She received the Laurea degree (*summa cum laude*) in biomedical engineering from the University of Rome "Tor Vergata," in 2005.

Since 2005, she has been a Contract Researcher with the Department of Civil Engineering, University of Rome "Tor Vergata." Her research interests include biomedical signal and image processing, physiopathological system modeling, biomechanics, homogenization, and Γ-convergence.